

Multi-objective optimal design of small scale resistance spot welding process with principal component analysis and response surface methodology

Dawei Zhao · Yuanxun Wang · Suning Sheng ·
Zongguo Lin

Received: 20 November 2012 / Accepted: 11 January 2013 / Published online: 26 January 2013
© Springer Science+Business Media New York 2013

Abstract This paper investigates the effects of welding parameters on the welding quality and optimizes them in the small scale resistance spot welding (SSRSW) process. Experiments are carried out on the basis of response surface methodology technique with different levels of welding parameters of spot welded titanium alloy sheets. Multiple quality characteristics, namely signal-to-noise (S/N) ratios of weld nugget diameter, penetration rate, tensile shear load and the failure energy, are converted into an independent quality index using principal component analysis. The mathematical model correlating process parameters and their interactions with the welding quality is established and discussed. And then this model is used to select the optimum process parameters to obtain the desired welding quality. The verification test results demonstrate that the method presented in this paper to optimize the welding parameters and enhance the welding performance is effective and feasible in the SSRSW process.

Keywords Small scale resistance spot welding · Response surface methodology · Multi-objective optimization method · Signal-to-noise ratio · Principal component analysis · Titanium alloy

Introduction

With the rapid development of microelectromechanical systems, small scale resistance spot welding (SSRSW) is commonly used in electronic and medical devices. Compared with normal scale or large scale resistance spot welding (LSRSW), SSRSW deals with relatively thinner sheet metal (sheet metal less than 0.2–0.5 mm) (Kaiser et al. 1982). SSRSW is distinct from LSRSW in many aspects; electrode sticking, expulsion, and non-repeatable welding may occur on condition of simply reducing welding parameters (Dong et al. 2002). There have been some studies on SSRSW. Zhou et al. (2000) investigate the weldability of thin sheet aluminum, brass, and copper in SSRSW. Ely and Zhou (2001) study the weldability of Kovar, steel, and nickel. Tan et al. (2004) expound the dynamic resistance during SSRSW of Ni sheets and point out that the dynamic resistance curve could be divided into six stages. Fukumoto et al. (2008) investigate the weldability of austenitic stainless steel. Xu and Zhai (2008) study the weldability of refractory alloy 50Mo-50Re thin sheet. Chen et al. (2012) adoptes a fully coupled thermal-electrical-mechanical finite element model (FEM) to provide a clearer understanding of the entire welding process and pointes out that the maximum electrode displacement and minimum dynamic resistance serve as important indicators of nugget quality which can directly reflect the formation and growth of nuggets during SSRSW.

Resistance spot welding (including SSRSW) is a complicated mechanical-thermal-electrical process and the weld quality is highly affected by various process conditions, noise and errors (Wen et al. 2009). However, there are few reports and literatures of the relevant studies on process optimization of SSRSW. Thus it is necessary to investigate an effective method to boost and optimize the quality of SSRSW.

D. Zhao (✉) · Y. Wang
Department of Mechanics, School of Civil Engineering
and Mechanics, Huazhong University of Science
and Technology, Wuhan 430074, China
e-mail: 641129789@qq.com

S. Sheng · Z. Lin
Grand Master Trading Limited, Miyachi Unitek Corporation,
Nanjing 211100, China

There are plentiful literature reports on process optimization in the RSW process. [Darwish and Al-Dekhial \(1999\)](#) propose response surface methodology (RSM) to explore the effects of spot welding parameters on the strength of spot welded aluminum sheets with commercial purity. The optimum process parameters for obtaining the desired spot welding quality are captured by the proposed polynomial mathematical model. [Rowlands and Antony \(2003\)](#) applies the Taguchi's loss function analysis to a spot welding process for the sake of discovering the key process parameter and RSM is also employed to identify the process parameters which affect the variability of the weld strength. Taguchi method is one of the simple and effective solutions for parameter design and experimental planning ([Siddiquee et al. 2010](#)). [Esme \(2009\)](#) applies Taguchi method to investigate the effects of welding parameters on the tensile shear strength in RSW process and obtains an optimum parameter combination for the maximum tensile shear strength by means of analyzing signal-to-noise (S/N) ratio. [Thakur and Nandedkar \(2010\)](#) recommend the Taguchi method to determine the effects of electrode force, welding current and welding time on the tensile shear strength of RSW of austenitic stainless steel. Analysis of variance is also performed to determine the predominant process parameters of RSW. [Khan et al. \(2012\)](#) develops a response surface model to study the influence of process parameters of weld-bonding on tensile shear strength of the weld-bond of 2 mm thick aluminum alloy sheets and discusses the effects of the significant process parameters and their interaction on the tensile shear strength. All these methods mentioned above have been proved to be satisfying by performing confirmatory tests afterwards. Whereas, all of these research reports only focus on one quality characteristic. It is well known that welding quality is commonly characterized by a number of indicators, such as nugget size, tensile shear strength, penetration rate and so on.

To overcome this shortcoming, the effects of spot welding parameters on multiple quality characteristics of RSW and resultful ideas on how to find the optimal welding parameters in a smart way are discussed in some research materials. [Antony \(2001\)](#) applies a Taguchi quality loss function to the RSW manufacturing process based on multi-objective optimization technique. It performs comparatively improvement in multiple quality characteristics compared with single quality characteristics by means of an example of electronic assembly problem. [Kim et al. \(2005\)](#) employs the RSM to establish the optimal input conditions to obtain a satisfactory weld quality of spot welded of highly tensile TRIP steel. [Muhammad et al. \(2012\)](#) applies a multi-objective optimization with simultaneous consideration of multiple response (radius of weld nugget and width of HAZ) using Taguchi method to optimize the multiple quality characteristics in RSW process. Experimental confirmation test is then carried out to validate that the predicted model is reliable. All the

optimization techniques mentioned above are on the basis of the assumption that the response values are uncorrelated or independent. But this may not be always reasonable in realistic situations ([Aslanlar 2006](#); [Sun et al. 2008](#)). Therefore, it is essential to eliminate the multi-colinearity problem prior to application of various optimization techniques.

Other process optimization methods are also proposed by some researchers. [Bai and Chai \(2012\)](#) investigate a hybrid intelligent optimal-setting control of the raw slurry blending process which can automatically adjust the set-points in order to respond to the variation of the boundary condition. The application results applied in an alumina factory in China prove the validity and effectiveness of the proposed methods. [Ding et al. \(2011\)](#) apply the traditional linear weighting methods, strength Pareto evolutionary algorithm (SPEA) and the K means supports vector clustering to achieve the multi-objective optimization design of the overall performance of injection molding machine. [Rani et al. \(2012\)](#) propose a modified genetic algorithm for the multi-objective optimization of PID controller parameters and the results show that it has the capability to optimally tune the PID controllers based on the nonlinear model of the pendulum. [Aghaei et al. \(2012\)](#) present a fuzzy optimization method to enhance the optimal power flow considering Unified Power Flow Controller. [Loghmanian et al. \(2012\)](#) propose a new modified elitist non-dominated sorting genetic algorithm using clustered crowding distance to minimize the complexity of a model structure and its predictive error simultaneously. All the methods mentioned above have not been employed in the field of spot welding, whereas an attempt may be made to improve the welding quality through using them for reference.

In the present work, first weld nugget size, tensile shear strength, penetration rate and failure energy are transformed into welding performance characteristics using signal-to-noise (S/N) ratio. And then the principal component analysis (PCA) is adopted to convert the four welding quality indices into an independent quality indicator. After eliminating the effects of multicollinearity among variables, RSM is employed to analyze and find out the optimal process parameters. Making use of the RSM modeling technique, the complicated relationships between the process parameters and the synthetical weld quality index of SSRSW are also discussed.

The rest of the paper is organized as follows. Section "Experimental detail" introduces the experimental conditions and experimental design. Section "Analysis methods and corresponding procedures" describes the methods and the corresponding procedures of the signal-to-noise (S/N) ratio method, PCA and RSM to obtain the composite welding quality index (CWQI) and the regression model quantifying the relationship between the input variables (welding current, welding time and welding force) and the output variable (CWQI). Section "The four principal component scores"

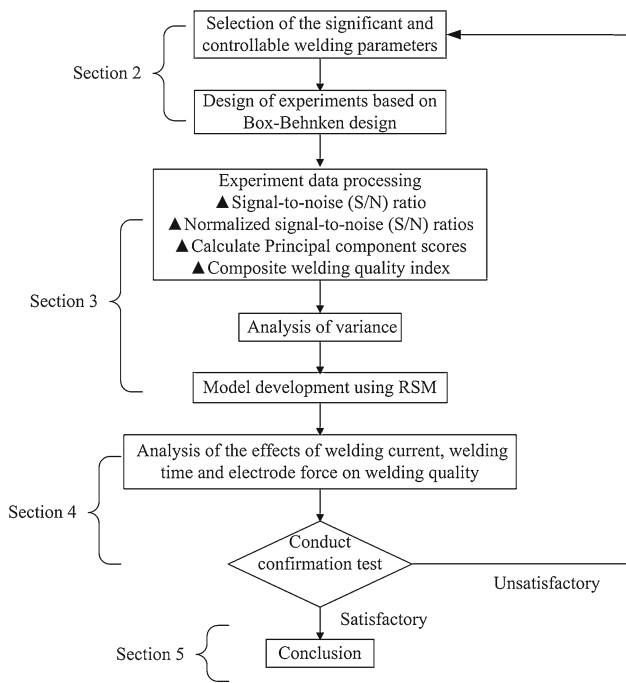


Fig. 1 The optimization procedures of the research methodology

discusses factor/interaction effects of welding parameters on *CWQI*, the optimizing design and experimental verification. Finally, Section “Conclusion” concludes the paper. The procedures applied in this research are shown in Fig. 1.

Experimental detail

Titanium and its alloys have been identified as one of the best engineering metals for application in many industrial fields (Kaya and Kahraman 2012), such as aviation, medical industry and chemical engineering, and so on. This is because titanium and titanium alloy have relatively low density, excellent corrosion resistance and high mechanical strength (Cui et al. 2011). Therefore, this paper is planned to optimize the welding parameters of TC2 titanium alloy sheets with the thicknesses of 0.4 mm. The alloy has satisfactory plasticity, good weldability and its chemical composition (percent by weight) is given in Table 1. The TC2 titanium alloy sheets are cut in the dimension of 100 × 30 × 0.4 mm, installed as lapping joints, as shown in Fig. 2.

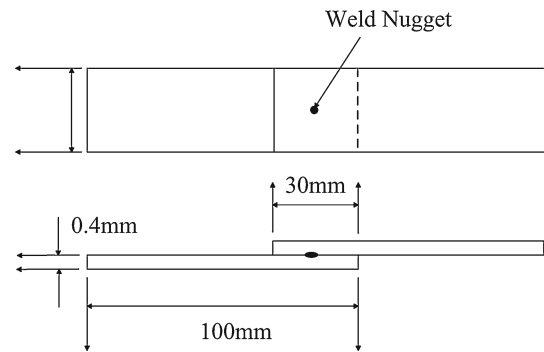


Fig. 2 Specimen sizes for SSRSW

When the temperature is higher than 550 °C, titanium and its alloy easily produce chemical reaction with oxygen, nitrogen, hydrogen, which reduces their performances. However, during resistance spot welding, under the pressure of electrodes the nugget does not directly contact with the air, so it does not require special protection measures. The rough degree and cleanness of metal sheet surfaces extremely affect the welding quality (Saresh et al. 2007), so it is necessary to reduce the surface resistance by mechanical and chemical methods before welding. In this research, first the sheets are cleaned using hard brush, and then are chemically cleaned by the mixed solution of 45 % of nitric acid, 20 % of hydrofluoric acid and 35 % of water. After etching for 2–3 min, the base metal sheets are cleaned with running water.

The spot welding tests are performed using a resistance spot weld machine produced by Miyachi Unitek Corporation. A HF27 high frequency resistance welding power supply with a pneumatically actuated small-scale resistance weld head is employed in this experiment. The HF27 power supply can provide constant current, constant voltage and constant power modes for a welding process. In this work constant current mode is used. The flatted copper alloy electrodes with 3 mm in diameter are employed. No cooling water is supplied to the electrodes.

In order to improve the reliability and availability of the test results, experiments are scheduled based on RSM technique. Box–Behnken designs (BBD) are a class of rotatable or nearly rotatable second-order designs based on three-level incomplete factorial designs (Souza et al. 2005; Ferreira et al. 2007), which are considered to be more suitable for the

Table 1 Chemical compositions of TC2 titanium alloy (wt%)

Alloying elements			Impurities (not more than)						
Al	Mn	Ti	Fe	C	N	H	O	Other elements	
								Single	Total
4.0	1.5	Remain	0.30	0.10	0.05	0.012	0.15	0.10	0.40

limited number of samples to be conducted in comparison with other experimental design methods (Beal et al. 2006). The 95 % confidence interval for the experimental results of the BBD is analyzed by default. In this paper, a BBD is finally chosen and the values of the welding process parameters at different levels are tabulated in Table 2.

The levels $-1, 0, 1$ in Table 2 are known as coded variables in the RSM, which are dimensionless, zero mean and the same standard deviation. Coded value of the variable welding time (T) z_1 is defined as (Muthukumar et al. 2003)

$$z_1 = (T - z_0)/\Delta z \quad (1)$$

where z_1 is the coded value of welding time, z_0 is the value of T at the center point, Δz is the step change of T , so as the welding current (I) and electrode force (F).

The number of experiments (N) required for the development of BBD is defined as (Ferreira et al. 2007):

$$N = 2q(q - 1) + C_0 \quad (2)$$

where q is number of factors and C_0 is the number of central points. In this paper, three factors (welding time, welding current and electrode force) are considered while $C_0 = 5$. The BBD can be viewed as consisting of three interlocking 2^2 factorial design and a central point (Souza et al. 2005; Aslan and Cebeci 2007), as shown in Fig. 3. The numbers in Fig. 3 are the experimental serial number conducted in this research; z_1, z_2 and z_3 are respectively coded welding time, welding current and electrode force.

After welding, tensile-shearing tests are carried out on a universal tensile testing machine with the tension speed of 1 mm/min. Nugget diameter is determined from the fractured faying surfaces of tensile-shear testing. The failure energy is extracted from the load-displacement curve and its value equals the curve area. As one of the most important factors governing the mechanical performance of resistance spot welds, penetration rate A is calculated according to the following formula:

$$A = h/(\delta - c) \times 100 \% \quad (3)$$

where h is the semiminor axis of the nugget; δ is the thickness of the plates to be welded; c is the indentation depth and D is the nugget diameter, as presented in Fig. 4. Table 3 illustrates the results of the experiments. The numbers in the brackets are the corresponding coded values of welding parameters.

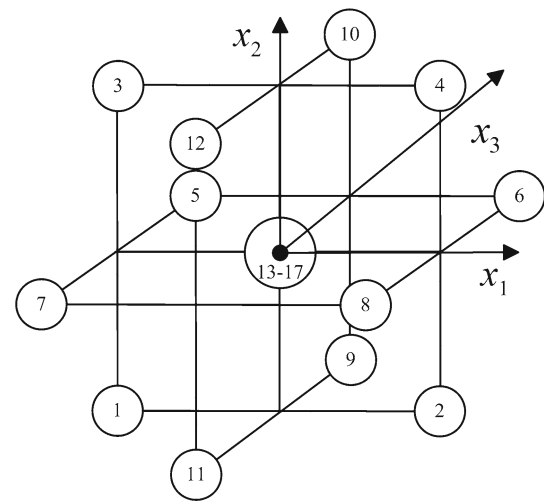


Fig. 3 The three-factorial Box–Behnken experimental design

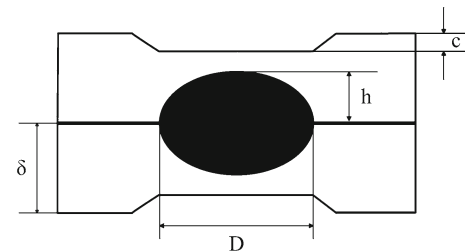


Fig. 4 Geometric morphology of the nugget

T, I, F respectively represents welding time, welding current and electrode force.

Analysis methods and corresponding procedures

Signal-to-noise ratio

As one of the simple and effective solutions for parameter design and experimental planning approach, signal-to-noise (S/N) ratio (Dubey and Yadava 2008) is employed to represent the welding performance characteristic in this study. There are three categories of the quality characteristics in the analysis of S/N ratio—the lower the better, the higher the better and the nominal the better.

Table 2 Welding process parameters at different levels

Symbol	Process parameter	Unit	Level -1	Level 0	Level 1
A	Welding time	ms	8	10	12
B	Welding current	kA	1.6	2.0	2.4
C	Electrode force	N	76.2	101.6	127

Table 3 Experimental results based on Box–Behnken design

Experiment number	Welding parameters			Nugget diameter (mm)	Penetration rate (%)	Shear strength (N)	Failure energy (J)
	<i>T</i>	<i>I</i>	<i>F</i>				
1	8 (−1)	1.6 (−1)	101.6 (0)	1.47	50.29	1395	1.68
2	12 (+1)	1.6 (−1)	101.6 (0)	1.67	58.35	1920	2.35
3	8 (−1)	2.4 (+1)	101.6 (0)	1.93	63.44	2206	2.62
4	12 (+1)	2.4 (+1)	101.6 (0)	2.18	64.78	2339	2.75
5	8 (−1)	2.0 (0)	76.2 (−1)	1.72	59.30	1996	2.32
6	12 (+1)	2.0 (0)	76.2 (−1)	2.05	65.04	2423	2.90
7	8 (−1)	2.0 (0)	127 (+1)	1.66	57.58	1893	2.25
8	12 (+1)	2.0 (0)	127 (+1)	1.78	61.14	2094	2.44
9	10 (0)	1.6 (−1)	76.2 (−1)	1.77	60.29	2075	2.55
10	10 (0)	2.4 (+1)	76.2 (−1)	2.16	63.24	2223	2.67
11	10 (0)	1.6 (−1)	127 (+1)	1.47	50.59	1400	1.76
12	10 (0)	2.4 (+1)	127 (+1)	2.07	67.92	2458	2.94
13	10 (0)	2.0 (0)	101.6 (0)	1.89	62.64	2187	2.54
14	10 (0)	2.0 (0)	101.6 (0)	1.88	62.74	2175	2.54
15	10 (0)	2.0 (0)	101.6 (0)	1.87	62.93	2187	2.54
16	10 (0)	2.0 (0)	101.6 (0)	1.87	62.23	2187	2.54
17	10 (0)	2.0 (0)	101.6 (0)	1.90	64.58	2175	2.54

The desired observed value of a lower-the-better characteristic is zero (Antony 2000). Examples include tool wear, noise level in automotive engines, response time to customer complaints, shrinkage porosity, warp and surface roughness (Antony 2000). The S/N ratio with a lower-the-better characteristic can be expressed as:

$$x_i = -10 \log \left(\frac{1}{n} \sum_{j=1}^n y_{ij}^2 \right) \tag{4}$$

where x_i is the S/N ratio; y_{ij} is the i th quality characteristic value at the j th test ($i = 1, 2, \dots, m; j = 1, 2, \dots, n$).

The larger-the-better response is generally employed when the objective of the experiment is to maximize the response value provided that it is within acceptable limits. Examples include strength, efficiency, miles/gallon of an automobile, corrosion resistance, product or component reliability, product life and so on (Antony 2000). The S/N ratio with a higher-the-better characteristic can be expressed as:

$$x_i = -10 \log \left(\frac{1}{n} \sum_{j=1}^n \frac{1}{y_{ij}^2} \right) \tag{5}$$

The nominal the better characteristic is recommended when the experimental objective is to achieve a target response value and a minimal variability around the target. Instances include dimensions (width, thickness, height, etc.), force, pressure, viscosity, resistance, voltage, current, capacitance

and so on (Antony 2000). The S/N ratio with the nominal the better characteristic can be expressed as:

$$x_i = 10 \log \left(\frac{\bar{y}_i^2}{\sigma_i^2} - \frac{1}{n} \right) \tag{6}$$

where $\bar{y}_i = \sum_{j=1}^n y_{ij}/n$ is the i th average quality characteristic experimental value; $\sigma_i^2 = \frac{1}{n-1} \sum_{j=1}^n (y_{ij} - \bar{y}_i)^2$ is the corresponding deviation and mn is the total number of the tests.

In this study, the penetration rate, tensile shear load and the failure energy are the higher the better characteristics; while the weld nugget size is the nominal the better characteristic. The S/N ratios for each experiment number are summarized in Table 4. The S/N ratios of penetration rate, tensile shear load and the failure energy in Table 4 are calculated from Eq. (5), and the S/N ratios of weld nugget size is obtained according to Eq. (6).

Principal component analysis

As an effective statistical technique, PCA is used in data compressing and statistical features extracting by means of eliminating the overlapping information of the samples, which changes high dimension into low dimension without much loss of information. The PCA method involves several procedures, as shown below (Fung and Kang 2005):

Table 4 The sequences of S/N ratios

Experiment number	S/N ratio (dB)			
	Nugget diameter	Penetration rate	Shear strength	Failure energy
1	56.44	78.36	144.81	10.38
2	65.19	81.33	151.20	17.09
3	96.63	83.00	153.98	19.26
4	47.96	83.42	155.15	20.23
5	67.94	81.65	151.98	16.83
6	103.87	83.50	155.86	21.29
7	61.57	81.06	150.92	16.22
8	71.06	82.26	152.94	17.84
9	69.02	81.98	152.75	18.72
10	49.37	82.94	154.13	19.64
11	57.84	78.47	144.89	11.31
12	100.44	84.37	156.14	21.57
13	88.00	82.75	153.81	18.64
14	85.67	82.78	153.70	18.64
15	75.21	82.84	153.81	18.96
16	76.30	82.75	153.81	18.49
17	92.77	82.62	153.70	18.49

1. The original multiple quality characteristic array

$$X = \begin{pmatrix} x_1(1) & \dots & x_1(n) \\ \vdots & \ddots & \vdots \\ x_m(1) & \dots & x_m(n) \end{pmatrix} \tag{7}$$

where m is the number of experiment and n is the number of the quality characteristic. In this paper, x is the S/N ratio of each quality characteristics and $m = 17, n = 4$.

2. Normalizing the response

The S/N ratio of each quality characteristic is normalized using the following formula to get rid of the differences between units.

$$x_i(j)^* = \frac{x_i(j) - x_i(j)^-}{x_i(j)^+ - x_i(j)^-} \tag{8}$$

$$X^* = \begin{pmatrix} x_1(1)^* & \dots & x_1(n)^* \\ \vdots & \ddots & \vdots \\ x_m(1)^* & \dots & x_m(n)^* \end{pmatrix} \tag{9}$$

where $x_i(j)^*$ is the normalized response, $x_i(j)^+$ is the maximum of $x_i(j)$, and $x_i(j)^-$ is the minimum of $x_i(j)$.

3. Correlation coefficient array

The correlation coefficient array is evaluated as follows:

$$R_{kl} = \frac{Cov(x_i(k)^*, x_i(l)^*)}{\sqrt{Var(x_i(k)^*)Var(x_i(l)^*)}} \tag{10}$$

$(k = 1, 2, 3, \dots, n; l = 1, 2, 3, \dots, n)$

where $Cov(x_i(k)^*, x_i(l)^*)$ is the covariance of sequences $x_i(k)^*$ and $x_i(l)^*$, $Var(x_i(k)^*)$ is the variance of sequence $x_i(k)^*$ and $Var(x_i(l)^*)$ is the variance of sequence $x_i(l)^*$, which represent the measures of quality characteristics k and l .

4. Determining the eigenvalues and eigenvectors

The eigenvalues and eigenvectors are determined from the correlation coefficient array,

$$(R - \lambda_k I_m) V_{ik} = 0 \tag{11}$$

where R is the matrix form of R_{kl} ; λ_k is the k th eigenvalue and $\sum_{k=1}^n \lambda_k = n, k = 1, 2, \dots, n$; $V_{ik} = [a_{k1} a_{k2} \dots a_{kn}]^T$ is the eigenvector corresponding to the eigenvalue λ_k .

5. Principal component scores

The principal component score $PCSi(k)$ corresponding to each trial condition is formulated as:

$$PCSi(k) = \sum_{j=1}^n x_i(j)^* \cdot V_{jk} \tag{12}$$

$(i = 1, 2, \dots, m; k = 1, 2, \dots, n)$

where $PCS_i(k)$ is the principal component score of the i th trial run in the k th quality characteristic, $x_i(j)^*$ is the corresponding normalized response, V_{jk} is the eigenvector corresponding to the eigenvalue λ_k , PCS is the matrix form of $PCS_i(k)$ and $PCS = [PCS(1), PCS(2), \dots, PCS(n)]$.

6. Evaluating the contribution rate and accumulating contribution rate of each principal component

$$AP_k = \frac{\lambda_k}{\sum_{k=1}^n \lambda_k} \quad (k = 1, 2, \dots, n) \tag{13}$$

$$AAP_k = \frac{\sum_{j=1}^k \lambda_j}{\sum_{k=1}^n \lambda_k} \quad (k = 1, 2, \dots, n) \tag{14}$$

where AP_k is the contribution rate, which explains the degree of the variation of the k th principal component. AAP_k is the accumulation contribution rate. In general, we select the top p ($p < n$) factors whose cumulative contribution of variance accounts to 85–95%.

Table 5 manifests that the first two principal components ($PC(1)$ and $PC(2)$) represent 99.52% of the variation in the responses. $PC(1)$ is able to explain about 83.22% of the total variation. Based on these statistical tests and indices, it might be postulated that only the first two principal component scores can be chosen to form the composite welding quality index ($CWQI$). The comprehensive index is defined as the sum of the products of the first two principle component scores multiplied by their corresponding eigenvalues. $CWQI = \sum_{k=1}^2 \lambda_k PCS(k)$ represents the original four welding quality indices and accounts for most of the variance in the original responses, as shown in Table 6. It is desirable to have a high $CWQI$. Through PCA, we synthesize four criteria, eliminate information overlapping of the sample, and reduce the dimension of welding quality indices.

Response surface methodology

RSM is a collection of statistical and mathematical method comprising of an experimental design for a polynomial

mathematical model between the input variables and output variables, the statistical modeling quantifying the relationships between the controllable input parameters and output variables (Beal et al. 2006), and the optimization of the response variables influenced by various process parameters, which are useful for the modeling and analyzing engineering problems. It is assumed that the independent input variables are continuous and controllable by experiments with negligible errors. By using the results of a numerical experiment in the points of BBD, response surface analysis is much less computationally expensive than conventional solution using the original method (Raissi and Farsani 2009). It is required to find a suitable approximation for the true functional relationship between independent variables and the response surface.

Generally, the relationship between the response variable y and the predictor variables (x_1, x_2, \dots, x_n) may be known exactly as a description (Lai et al. 2009):

$$y = f(x_1, x_2, \dots, x_n) + \varepsilon \tag{15}$$

where ε is model error and includes measurement error and other variability.

In this study, $f(x_1, x_2, \dots, x_n)$ is a function of the welding parameters such as welding time (T), welding current (I), and electrode force (F), which quantifies the $CWQI$ of spot-welded TC2 titanium alloy. The function can be expressed as:

$$f(x_1, x_2, \dots, x_n) = g(x_1, x_2, \dots, x_n) + \varepsilon \tag{16}$$

where $g(x_1, x_2, \dots, x_n)$ is the polynomial of order three or less.

The successful application of RSM relies on the identification of a suitable and precise approximation for $g(x_1, x_2, \dots, x_n)$. The second-order polynomial (regression) equation used to represent the function $g(x_1, x_2, \dots, x_n)$ is given by:

Table 5 Principal component analysis of the original S/N ratio responses

Item	Principal components			
	<i>PC(1)</i>	<i>PC(2)</i>	<i>PC(3)</i>	<i>PC(4)</i>
Eigenvalues	3.3289	0.6518	0.0141	0.0052
Proportion	0.8322	0.1630	0.0035	0.0013
Accumulated proportion	0.8322	0.9952	0.9987	1.0000
Responses (S/N ratio)	Eigenvectors			
Nugget diameter	0.3609	−0.9322	−0.0259	−0.0106
Penetration rate	0.5400	0.1856	0.6252	0.5320
Shear strength	0.5389	0.2156	0.1524	−0.8005
Failure energy	0.5365	0.2258	−0.7650	0.2757

Table 6 Four principal component scores and the composite welding quality index

No.	<i>PCS(1)</i>	<i>PCS(2)</i>	<i>PCS(3)</i>	<i>PCS(4)</i>	$\lambda_1 \cdot PCS(1)$	$\lambda_2 \cdot PCS(2)$	<i>CWQI</i>
1	0.0548	-0.1415	-0.0039	-0.00161	0.1824	-0.0923	0.0902
2	1.0039	0.0604	-0.0715	-0.02617	3.3420	0.0394	3.3813
3	1.5935	-0.3158	-0.0234	-0.02672	5.3045	-0.2058	5.0986
4	1.4190	0.5500	-0.0078	-0.03934	4.7237	0.3585	5.0823
5	1.0753	0.0339	-0.0112	-0.05929	3.5797	0.0221	3.6018
6	1.8716	-0.3449	-0.0885	-0.06657	6.2303	-0.2248	6.0055
7	0.9015	0.0897	-0.0419	-0.05041	3.0011	0.0584	3.0595
8	1.2443	0.0392	-0.0051	-0.04867	4.1422	0.0255	4.1677
9	1.2396	0.0790	-0.0960	-0.03847	4.1264	0.0515	4.1779
10	1.3082	0.4806	-0.0318	-0.02487	4.3549	0.3132	4.6681
11	0.1225	-0.1410	-0.0548	0.026513	0.4078	-0.0919	0.3159
12	1.9541	-0.2500	-0.0116	-0.00273	6.5049	-0.1630	6.3419
13	1.4770	-0.1957	-0.0057	-0.0506	4.9169	-0.1275	4.7894
14	1.4596	-0.1579	-0.0028	-0.03956	4.8590	-0.1029	4.7561
15	1.4178	0.0267	-0.0116	-0.0323	4.7196	0.0174	4.7370
16	1.3940	-0.0039	0.0105	-0.05227	4.6404	-0.0025	4.6379
17	1.4832	-0.2844	-0.0123	-0.05925	4.9373	-0.1854	4.7520

$$g(x_1, x_2, \dots, x_n) = a_0 + \sum_{i=1}^n a_i x_i + \sum_{i=1}^n a_{ii} x_i^2 + \sum_{j \neq i}^n a_{ij} x_i x_j + \varepsilon \quad (17)$$

where x_i denotes the coded unit of the input variables, and $g(x_1, x_2, \dots, x_n)$ is the output variable. In addition, a_0 is the average of the responses and a_i, a_{ij}, a_{ii} are regression coefficients that depend on respective linear, interaction, and squared terms of factors, which are obtained from the experimental result data using least square method.

The Design Expert Software is employed to determine the regression coefficients and analysis of variance (ANOVA) with all factors and their respective values is also performed, as listed in Table 7. In this study, T, I, F, TI, TF, IF, T^2 and I^2 are significant factors as the P values of them are much smaller than 0.05. Correspondingly, the P value of model term F^2 is greater than 0.10 which indicates that it is not significant. Besides, the full quadratic model is also significant since its P value is below 0.05. The lack of fit F value is 1.65 implying that the lack of fit is insignificant relative to the pure error. There is a 31.22% chance that a lack of fit F value this large could occur due to noise. Non-significant lack of fit is good—we want the model to fit.

The fitting degree of the theoretical quadratic polynomial regression model is examined by the determination coefficient, as listed in Table 8. The coefficient of determination R^2 is 0.9993 for response, which implies that 99.93% of experimental data confirm the compatibility with the data predicted

by the model and the model can not explain only 0.07% of the total variations. The R^2 value is always between 0 and 1, and its value indicates capability of the model. With regard to a good statistical model, R^2 value should be close to 1.0 (Karthikeyan and Balasubramanian 2010). The adjusted R^2 value reconfigures the analytic expression with the significant terms. The value of the adjusted determination coefficient (Adjusted $R^2 = 0.9985$) is also big enough to support the high significance of the model. The predicted R^2 is 0.9938 indicates that the model is able to explain 99.38% of the variability in predicting completely new experimental data. This is in reasonable agreement with the adjusted R^2 of 0.9985. The value of coefficient of variation is as low as 1.58, which reveals that the deviations between experimental and predicted values are low. Adeq precision meant the signal to noise ratio. A ratio greater than 4 is desirable. In this investigation, the ratio is 125.862, which indicates an adequate signal. This model is able to navigate the design space. Figure 5 presents the accuracy of the predicted $CWQI$ and the measured $CWQI$. The straight line in Fig. 5 is a 45 degree line. The predicted $CWQI$ and the measured $CWQI$ are aligned, which once again favors the robustness and flexibility of the mathematical model.

As the quadratic factor F^2 has little effect on the model (with a P value of 0.3521), presents low effect, this less significant source can be excluded from the regression analysis. Based on this analysis, the regression coefficients for the estimation of $CWQI$ are decided and the equation of the fitted regression model is achieved as follows:

Table 7 ANOVA test results

Source	Sum of squares	df	Mean square	F value	P value Prob > F
Model	45.19	9	5.02	1195.07	<0.0001
T	5.76	1	5.76	1370.20	<0.0001
I	21.86	1	21.86	5203.45	<0.0001
F	2.61	1	2.61	620.79	<0.0001
TI	2.73	1	2.73	650.87	<0.0001
TF	0.42	1	0.42	99.86	<0.0001
IF	7.66	1	7.66	1823.27	<0.0001
T ²	1.03	1	1.03	244.87	<0.0001
I ²	2.88	1	2.88	685.37	<0.0001
F ²	0.004175	1	0.004175	0.99	0.3521
Residual	0.029	7	0.004202		
Lack of fit	0.016	3	0.005429	1.65	0.3122
Pure error	0.013	4	0.003282		
Cor total	45.22	16			

Table 8 Post-ANOVA statistics

Standard deviation	0.065	R-squared	0.9993
Mean	4.10	Adjusted R-squared	0.9985
Coefficient of variation (%)	1.58	Predicted R-squared	0.9938
Predicted residual sum of squares	0.28	Adeq precision	125.862

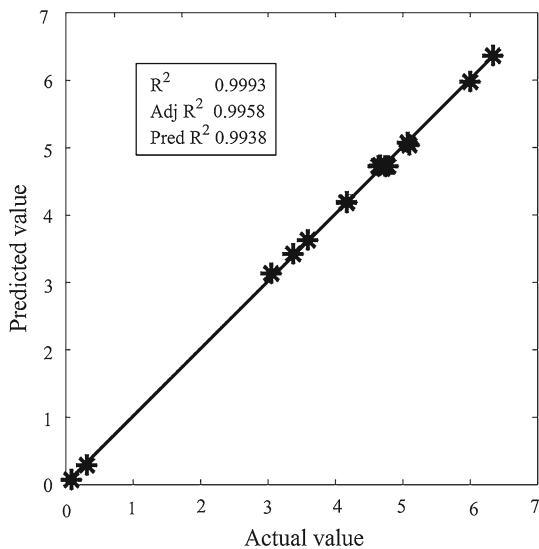


Fig. 5 Accuracy of the predicted *CWQI* and the measured *CWQI*

$$\begin{aligned}
 CWQI = & -38.09029 + 5.61913T + 21.34668I - 0.23115F \\
 & - 1.03360TI - 0.00637583TF + 0.13622IF \\
 & - 0.124T^2 - 5.17929I^2 \quad (18)
 \end{aligned}$$

The equation is valid under the following conditions:

$$\begin{aligned}
 8 \leq T \leq 12 \\
 1.6 \leq I \leq 2.4 \\
 76.2 \leq F \leq 127
 \end{aligned} \quad (19)$$

Accordingly, the regression model with the coded welding parameters is:

$$\begin{aligned}
 CWQI = & 4.72 + 0.85z_1 + 1.65z_2 - 0.57z_3 - 0.83z_1z_2 \\
 & - 0.32z_1z_3 + 1.38z_2z_3 - 0.5z_1^2 - 0.83z_2^2 \quad (20)
 \end{aligned}$$

The equation is valid under the following conditions:

$$\begin{aligned}
 -1 \leq z_1 \leq 1 \\
 -1 \leq z_2 \leq 1 \\
 -1 \leq z_3 \leq 1
 \end{aligned} \quad (21)$$

where z_1 is the coded welding time, z_2 is the coded welding current and z_3 is the coded electrode force.

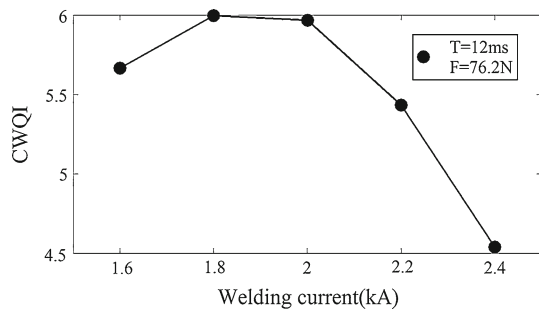


Fig. 6 Effect of welding current on *CWQI*

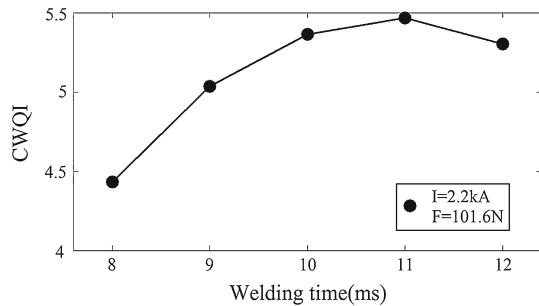


Fig. 7 Effect of welding time on *CWQI*

Overall results and discussion

Effects of welding parameters on *CWQI*

Plots of each factor and its effect on *CWQI* are presented in Figs. 6, 7 and 8. In order to avoid errors, all the factors and interactions must be considered carefully. In each of these graphs, the factors that are not plotted are kept at certain constant values. The figures indicate that all the welding parameters highly affect the *CWQI*.

Figure 6 shows the effect of welding current on the *CWQI*. It can be observed that the *CWQI* of the spot-welded joint increases with the welding current increasing from 1.6 to 2 kA, then it decreases with further increase of welding (2–2.4 kA). As the welding current increases, the heat generated at the faying surface of the welding plates is increased and therefore the nugget diameter is also increased; which in turn results in higher tensile shear strength of the weld joint. When the welding heat continues to increase, the heating rate of the materials is higher than normal and the materials expand faster. As the welding heat input exceeds a certain value, expulsion is prone to occur, which leads to the eruption of the molten metal from the nugget during welding. The occurrence of expulsion would reduce the welding surface quality, affect its corrosion resistance, mechanical properties and fatigue strength, shorten the electrode service life (Senkara et al. 2004), which should be avoided.

Different *CWQI* with the welding time varying from 8 to 12 ms are presented in Fig. 7. From the figure we can see

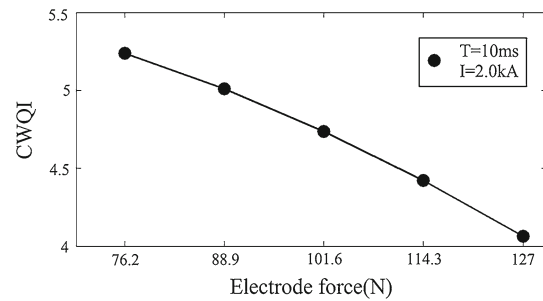


Fig. 8 Effect of electrode force on *CWQI*

that as welding time gets longer, the *CWQI* of the weld bond first increases from 4.43 to 5.47 then decreases with further increase of welding time. According to the joule law ($Q = I^2 R t$), longer welding time indicates larger welding heat input, which means that the nugget grows adequately and the mechanical properties of the joints increases. Nevertheless, welding time longer than a certain value is unacceptable, especially with larger current. Overlong welding time combining with larger current leads mechanical collapse surrounding the weld nugget, which reduces the *CWQI*. From what has been mentioned above, effect of welding time on the welding quality is similar to that of welding current.

Figure 8 examines the effect of electrode force on *CWQI* visually. As electrode force increases, the *CWQI* get reduced. This variation is due to the fact that the electrode force causes the faying surface collapse and changes the contact area, which in turn changes the contact resistance. As the electrode force increases, a larger metallic contact area will be generated and this leads to a lower contact resistance at the faying surface. Consequently, the heat generation at the interface is reduced and the nugget diameter is smaller compared with lower electrode force. In addition, the electrode force affects the weld current thresholds for nugget initiation in SSRSW; that is to say, as the electrode force increases, the minimum critical welding current needed to form the welding nugget is correspondingly lower and vice versa. It should be pointed out that the electrode force must be high enough to produce a comparatively acceptable nugget, but still low enough to deform of the faying surface asperities without metal expulsion or electrode sticking; as the basic process of expulsion can be described by the interaction between the forces from the liquid nugget and its surrounding solid containment (Senkara et al. 2004).

The extent of the process parameters impact of the *CWQI* can be ranked from their respective F ratio values (Lakshiminarayanan and Balasubramanian 2009) as well as the regression coefficients in Eq. (20). As the degrees of freedom of all the input parameters are identical, a higher F ratio value implies that the corresponding factor is more significant than others and vice versa. From the F ratio values listed in Table 7, it can be seen that welding current contributes more

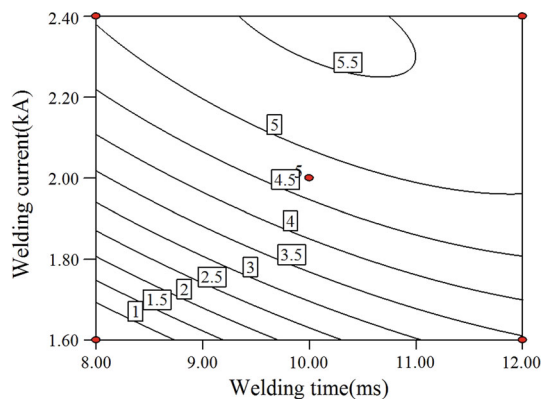


Fig. 9 Contour plots with the electrode force kept at 101.6 N

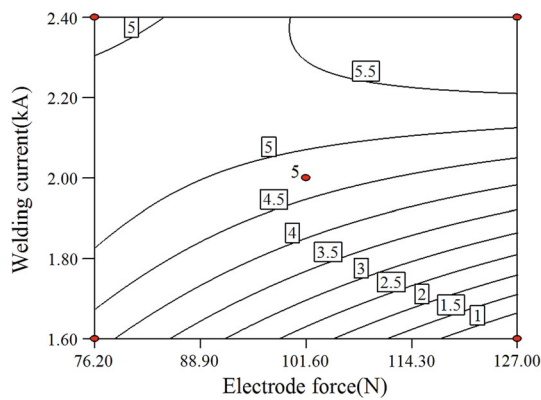


Fig. 10 Contour plots with the welding time kept at 10 ms

on *CWQI*, followed by welding time and electrode force for the range considered in this investigation.

Interaction effect of welding parameters

Contour plot plays a very important role in the study of a response surface. To reveal the interaction effects of welding parameters on *CWQI* and find the optimized combination of the welding process parameters of *CWQI*, the contour plots are presented in Figs. 9, 10 and 11. The contour plots are obtained through setting one parameter as a certain constant value while the other two variables vary in the range considered in this paper. The values in the boxes of Figs. 9, 10 and 11 are different *CWQI* with different welding parameters.

Figures 9, 10 and 11 respectively reveals the interaction effects of three welding process parameters on the welding quality. The contours indicate that the optimal welding can be achieved under relatively higher welding current accompanying with larger electrode force. When the electrode pressure is constant, it is beneficial to employ larger

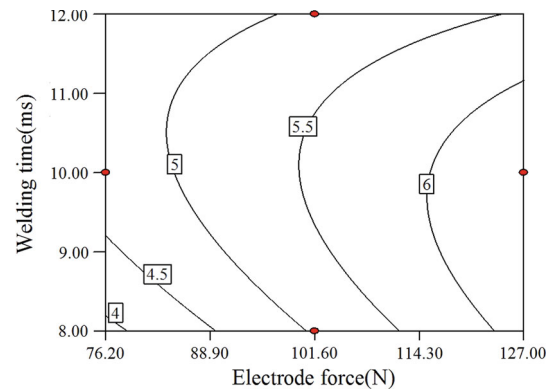


Fig. 11 Contour plots with the welding current kept at 2.4 kA

welding current and appropriate welding time; the welding time should not be too large, otherwise it may result in expulsion, but also not too small, or the nugget grows limitedly, fails to reach its maximum mechanical properties. Thus it can be seen that the specific combination of welding process parameters may target a certain given welding quality index. The contour maps of different welding qualities with various combinations of welding process parameters could provide a guidance opinion to constitute process scheme based on production requirements.

From the *F* ratio values listed in Table 7 as well as the regression coefficients in Eq. (20). It can be concluded that the interaction effect between welding current and electrode force (*IF*) affects more significantly on welding quality as compared to that of interactions between welding current and welding time (*TI*) and welding time and electrode force (*TF*).

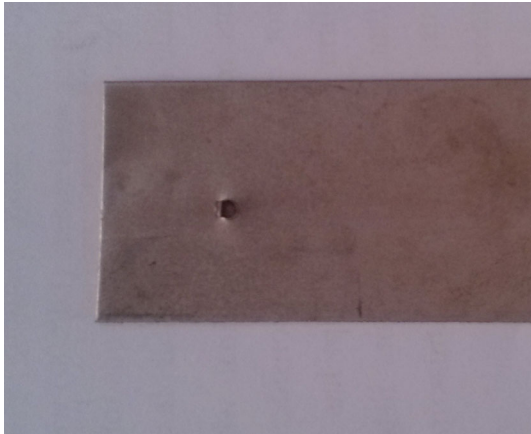
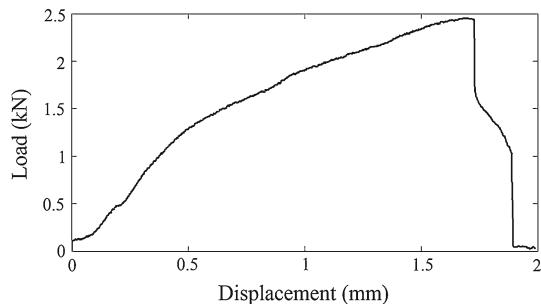
Optimizing design and experimental verification

Generally speaking, as for multi-response performance optimization problem, each response variable value must be computed and the factor/interaction effects which significantly influence the multi-response performance must be considered. However, in this investigation the multi-response performance statistic can be treated as an individual response after a series of pretreatment described previously.

In order to optimize the response, the desirability function (Islam et al. 2009) is employed using Design Expert software version 8.0.6. There are many methods available to optimize a process. In this work, numerical optimization is chosen (Hameed et al. 2009). Numerical optimization presents a comprehensive and up-to-date description of the most effective methods in continuous optimization. The value of desirability function is always between 0 and 1. With regard to the optimal welding parameters, it should be as large as possible. The goal seeking begins at a random starting point and proceeds up the steepest slope to a maximum.

Table 9 Different welding parameters with different desirability function values

Welding time (ms)	Welding current (kA)	Electrode force (N)	<i>CWQI</i>	Desirability function value
9.39	2.4	127	6.40474	0.914
9.45	2.4	127	6.40436	0.914
9.47	2.4	125.51	6.35118	0.906
12.00	1.98	76.70	5.97087	0.851

**Fig. 12** The failure characteristic of the welded sample with the optimum welding parameters**Fig. 13** The tensile-shearing curve of the specimen joined with the optimum welding parameters

There may be two or more maximums because of curvature in the response surfaces and their combination into the desirability function. By starting from several points in the design space chances improve for finding the “best” local maximum (Olmez 2009).

For the sake of getting the global optimal parameters, the optimal combination of welding parameters is the one yielding the maximum desirability function value together with the biggest *CWQI* value and the variables of welding time, welding current and electrode force are selected to be within the range considered in this paper, as shown in Table 9. The maximum achievable *CWQI* value is found to be 6.40474 through response surface analysis. The corresponding parameters that yield this maximum value are respectively welding time of 9.39 ms, welding current of 2.4 kA, and electrode force of 127 N.

The confirmation experiment is a crucial step to verify the feasibility and reproducibility of the experimental conclusions. If the confirmatory experiment results are persuasive, the proposed method is effective and significant in a specific productive field. On the other hand, if unsatisfactory results are obtained, further investigation of the problem may be required. The verification test is implemented with a specific combination of the factors previously evaluated. In this study, after determining the optimum conditions and predicting the response under these conditions, tests are carried out with the optimal welding parameters to determine the nugget diameter, penetration rate, shear strength and failure energy. The macrograph of failure characteristic of the welded sample with the optimal welding parameters is presented in Fig. 12. It can be seen that the failure mode of the welded joint is pullout failure. Failure mode has a significant influence on the peak load and failure energy of the spot welds and a pullout failure mode is most desirable (Hernandez et al. 2008). Figure 13 gives the tensile-shearing curve of the specimen joined at the predetermined welding time, welding current and electrode force. The shear strength is about 2,450 N and the failure energy is 2.96 J. The experimental results presented in Table 10 are encouragingly satisfactory, which proves that the parameter combination obtained by the

Table 10 Results of the confirmation experiment

Welding time (ms)	Welding current (kA)	Electrode force (N)	Nugget diameter (mm)	Penetration rate (%)	Shear strength (N)	Failure energy (J)	<i>CWQI</i>
9.39	2.4	127	2.05	67.45	2450	2.96	6.40474

proposed approach performs well for multi-quality characteristic optimization problem.

Conclusions

This work presents a multi-objective optimization technique based on PCA and RSM to study a SSRSW process with four correlated responses. First a Box–Behnken experimental designs which require smaller number of experiments is chosen and the corresponding nugget diameter, penetration rate, shears strength and failure energy are obtained. Then the four observed values are transformed into the welding performance characteristics through signal-to-noise (S/N) ratio. The first two principal component scores are chosen to form the CWQI after PCA, which converts the multi-response performance statistics into an individual response value. A regression model is obtained from the experimental data to quantify the relationship between the input variables (welding current, welding time and welding force) and the output variable (CWQI) which is a converged by the principal component scores using the first and second eigenvalues as weights. The variance of each principal component is taken as the weight to obtain the CQWI, which eliminates drawbacks of man-made subjectivism. The contour plots are displayed and the effects of welding parameters on CWQI are also discussed. Larger electrode force together with appropriate welding time and welding current is desirable. Though all the three input variables affect the CWQI, analysis of variance indicates that welding current contributes more on CWQI, followed by welding time and electrode force. In order to avoid the possibility that the optimal parameters are not global within the range considered in this paper, the optimal combination of welding parameters is the one yielding the maximum desirability function value together with the biggest CWQI value. The result of verification test which is performed with overall optimum welding parameters determined through the response surface method proves that the proposed approach is effective and feasible for a SSRSW process, which might be used as a valuable reference for optimizing and promoting welding quality of SSRSW in a mass production line.

The proposed approach for multi-quality characteristic optimization problem would perform well in some other relevant field so long as all of the responses of the multi-response problem are not independent of each other. The only thing we should do is to select the significant and controllable factors and obtain the new correlative responses through experiments when dealing with process optimization problems of this sort. The correlation coefficient can be calculated for checking the relationship between the performance indicators.

Acknowledgments The authors are grateful for the financial supported by the National Natural Science Foundation of China (11072083) and the Chinese Universities Scientific Fund (C2009M002). The authors are also grateful for the experiment supported by the analysis and test centre of Huazhong University of Science and Technology and Dongfeng Peugeot Citroen Automobile Company Limited.

References

- Aghaei, J., Ara, A. L., & Shabani, M. (2012). Fuzzy multi-objective optimal power flow considering UPFC. *International Journal of Innovative Computing, Information and Control*, 8, 1155–1166.
- Antony, J. (2000). Multi-response optimization in industrial experiments using Taguchi's quality loss function and principal component analysis. *Quality and Reliability Engineering International*, 16, 3–8.
- Antony, J. (2001). Simultaneous optimization of multiple quality characteristics in manufacturing processes using Taguchi's Quality Loss Function. *International Journal of Advanced Manufacturing Technology*, 17, 134–138.
- Aslan, N., & Cebeci, Y. (2007). Application of Box–Behnken design and response surface methodology for modeling of some Turkish coals. *Fuel*, 86, 90–97.
- Aslanlar, S. (2006). The effect of nucleus size on mechanical properties in electrical resistance spot welding of sheets used in automotive industry. *Materials & Design*, 27, 125–131.
- Bai, R., & Chai, T. (2012). Hybrid intelligent optimal-setting control with multi-objectives of the raw slurry blending process in the alumina production. *International Journal of Innovative Computing, Information and Control*, 8, 1251–1262.
- Beal, V. E., Erasenthiran, P., Hopkinson, N., Dickens, P., & Ahrens, C. H. (2006). Optimization of processing parameters in laser fused H13/Cu materials using response surface method (RSM). *Journal of Materials Processing Technology*, 174, 145–154.
- Chen, Y. C., Tseng, K. H., & Cheng, Y. S. (2012). Electrode displacement and dynamic resistance during small-scale resistance spot welding. *Advanced Science Letters*, 11, 72–79.
- Cui, C., Hu, B. M., Zhao, L., & Liu, S. (2011). Titanium alloy production technology, market prospects and industry development. *Materials & Design*, 32, 1684–1691.
- Darwish, S. M., & Al-Dekhial, S. D. (1999). Statistical models for spot welding of commercial aluminum sheets. *International Journal of Machine Tools and Manufacture*, 39, 1589–1610.
- Ding, L., Tan, J., Wei, Z., Chen, W., & Gao, Z. (2011). Multi-objective performance design of injection molding machine via a new multi-objective optimization algorithm. *International Journal of Innovative Computing, Information and Control*, 7, 3939–3950.
- Dong, S. J., Kelkar, G. P., & Zhou, Y. (2002). Electrode sticking during micro-resistance welding of thin metal sheets. *IEEE Transactions on Electronics Packaging Manufacturing*, 25, 355–361.
- Dubey, A. K., & Yadava, V. (2008). Robust parameter design and multi-objective optimization of laser beam cutting for aluminium alloy sheet. *The International Journal of Advanced Manufacturing Technology*, 38, 268–277.
- Ely, K. J., & Zhou, Y. (2001). Microresistance spot welding of Kovar, steel, and nickel. *Science and Technology of Welding & Joining*, 6, 63–72.
- Esme, U. (2009). Application of Taguchi method for the optimization of resistance spot welding process. *The Arabian Journal for Science and Engineering*, 34, 519–528.
- Ferreira, S. L. C., Bruns, R. E., Ferreira, H. S., Matos, G. D., David, J. M., Brandao, G. C., et al. (2007). Box-Behnken design: An alternative for the optimization of analytical methods. *Analytica Chimica Acta*, 597, 179–186.

- Fukumoto, S., Fujiwara, K., Toji, S., & Yamamoto, A. (2008). Small-scale resistance spot welding of austenitic stainless steels. *Materials Science and Engineering A*, 492, 243–249.
- Fung, H. C., & Kang, P. C. (2005). Multi-response optimization in friction properties of PBT composites using Taguchi method and principal component analysis. *Journal of Materials Processing Technology*, 170, 602–610.
- Hameed, B. H., Lai, L. F., & Chin, L. H. (2009). Production of biodiesel from palm oil (*Elaeis guineensis*) using heterogeneous catalyst: An optimized process. *Fuel Processing Technology*, 90, 606–610.
- Hernandez, V. H. B., Kuntz, M. L., Khan, M. I., & Zhou, Y. (2008). Influence of microstructure and weld size on the mechanical behavior of dissimilar AHSS resistance spot welds. *Science and Technology of Welding and Joining*, 13, 769–776.
- Islam, M. A., Sakkas, V., & Albanis, T. A. (2009). Application of statistical design of experiment with desirability function for the removal of organophosphorus pesticide from aqueous solution by low-cost material. *Journal of Hazardous Materials*, 170, 230–238.
- Kaiser, J. G., Dunn, G. J., & Eagar, T. W. (1982). Effect of electrical resistance on nugget formation during spot welding. *Welding Journal*, 62, 167s–174s.
- Karthikeyan, R., & Balasubramanian, V. (2010). Predictions of the optimized friction stir spot welding process parameters for joining AA2024 aluminum alloy using RSM. *International Journal of Advanced Manufacturing Technology*, 51, 173–183.
- Kaya, Y., & Kahraman, N. (2012). The effects of electrode force, welding current and welding time on the resistance spot weldability of pure titanium. *International Journal of Advanced Manufacturing Technology*, 60, 127–134.
- Khan, F., Dwivedi, M. D., & Sharma, S. (2012). Development of response surface model for tensile shear strength of weld-bonds of aluminium alloy 6061 T651. *Materials & Design*, 34, 673–678.
- Kim, T., Park, H., & Rhee, S. (2005). Optimization of welding parameters for resistance spot welding of TRIP steel with response surface methodology. *International Journal of Production Research*, 43, 4643–4657.
- Lai, X. M., Luo, A. H., Zhang, Y. S., & Chen, G. L. (2009). Optimal design of electrode cooling system for resistance spot welding with the response surface method. *International Journal of Advanced Manufacturing Technology*, 41, 226–233.
- Lakshminarayanan, A. K., & Balasubramanian, V. (2009). Comparison of RSM with ANN in predicting tensile strength of friction stir welded AA7039 aluminum alloy joints. *Transactions of Nonferrous Metals Society of China*, 19, 9–18.
- Loghmanian, S. M. R., Yusof, R., Khalid, M., & Ismail, F. S. (2012). Polynomial NARX model structure optimization using multi-objective genetic algorithm. *International Journal of Innovative Computing, Information and Control*, 8, 7341–7362.
- Muhammad, N., Manurung, Y. H. P., Jaafar, R., Abas, S. K., Tham, G., & Haruman, E. (2012). Model development for quality features of resistance spot welding using multi-objective Taguchi method and response surface methodology. *Journal of Intelligent Manufacturing*. doi:10.1007/s10845-012-0648-3
- Muthukumar, M., Mohan, D., & Rajendran, M. (2003). Optimization of mix proportions of mineral aggregates using Box Behnken design of experiments. *Cement & Concrete Composites*, 25, 751–758.
- Olmez, T. (2009). The optimization of Cr (VI) reduction and removal by electrocoagulation using response surface methodology. *Journal of Hazardous Materials*, 162, 1371–1378.
- Raissi, S., & Farsani, R. E. (2009). Statistical process optimization through multi-response surface methodology. *World Academy of Science, Engineering and Technology*, 51, 267–271.
- Rani, M. R., Selamat, H., Zamzuri, H., & Ibrahim, Z. (2012). Multi-objective optimization for PID controller tuning using the global ranking genetic algorithm. *International Journal of Innovative Computing, Information and Control*, 8, 269–284.
- Rowlands, H., & Antony, J. (2003). Application of design of experiments to a spot welding process. *Assembly Automation*, 23, 273–279.
- Saresh, N., Pillai, M. G., & Mathew, J. (2007). Investigations into the effects of electron beam welding on thick Ti-6Al-4V titanium alloy. *Journal of Materials Processing Technology*, 192–93, 83–88.
- Senkara, J., Zhang, H., & Hu, S. J. (2004). Expulsion prediction in resistance spot welding. *Welding Journal*, 83, 123s–132s.
- Siddiquee, A. N., Khan, Z. A., & Mallick, Z. (2010). Grey relational analysis coupled with principal component analysis for optimization design of the process parameters in in-feed centreless cylindrical grinding. *International Journal of Advanced Manufacturing Technology*, 46, 983–992.
- Souza, A. S., Dos Santos, W. N. L., & Ferreira, S. L. C. (2005). Application of Box-Behnken design in the optimization of an on-line pre-concentration system using knotted reactor for cadmium determination by flame atomic absorption spectrometry. *Spectrochimica Acta Part B: Atomic Spectroscopy*, 60, 737–742.
- Sun, X., Stephens, E. V., & Khaleel, M. A. (2008). Effects of fusion zone size and failure mode on peak load and energy absorption of advanced high strength steel spot welds under lap shear loading conditions. *Engineering Failure Analysis*, 15, 356–367.
- Tan, W., Zhou, Y., Kerr, H. W., & Lawson, S. (2004). A study of dynamic resistance during small scale resistance spot welding of thin Ni sheets. *Journal of Physics D: Applied Physics*, 37, 1998–2008.
- Thakur, A. G., & Nandedkar, V. M. (2010). Application of Taguchi method to determine resistance spot welding conditions of austenitic stainless steel AISI 304. *Journal of Scientific & Industrial Research*, 69, 680–683.
- Wen, J., Wang, C. S., Xu, G. C., & Zhang, X. Q. (2009). Real time monitoring weld quality of resistance spot welding for stainless steel. *ISIJ International*, 49, 553–556.
- Xu, J., & Zhai, T. (2008). The small-scale resistance spot welding of refractory alloy 50Mo-50Re thin sheet. *JOM Journal of the Minerals, Metals and Materials society*, 60, 80–83.
- Zhou, Y., Gorman, P., Tan, W., & Ely, K. J. (2000). Weldability of thin sheet metals during small-scale resistance spot welding using an alternating-current power supply. *Journal of Electronic Materials*, 29, 1090–1099.